Colloids and Surfaces B: Biointerfaces 117 (2014) 267–276

Contents lists available at ScienceDirect

Colloids and Surfaces B: Biointerfaces

journal homepage: www.elsevier.com/locate/colsurfb

ZnO nanoparticles induced oxidative stress and apoptosis in HepG2 and MCF-7 cancer cells and their antibacterial activity

Rizwan Wahab[a,*], Maqsood A. Siddiqui[a], Quaiser Saquib[a], Sourabh Dwivedi[a], Javed Ahmad[a], Javed Musarrat[b], Abdulaziz A. Al-Khedhairy[a], Hyung-Shik Shin[c]

[a] A.R. Al-Jeraisy Chair for DNA Research, College of Science, Department of Zoology, King Saud University, Riyadh 11451, Saudi Arabia
[b] Department of Agricultural Microbiology, Faculty of Agricultural Sciences, Aligarh Muslim University, Aligarh 202002, India
[c] Energy Materials and Surface Science Laboratory, Solar Energy Research Centre, School of Chemical Engineering, Chonbuk National University, Jeonju 561-756, Republic of Korea

ARTICLE INFO

Article history:
Received 13 September 2013
Received in revised form 19 February 2014
Accepted 22 February 2014
Available online 2 March 2014

Keywords:
X-ray diffraction pattern (XRD)
HepG2 and MCF-7 cancer cells
MTT
Flow cytometry
ZnO nanoparticles

ABSTRACT

Liver and breast cancer are the most traumatic diseases because they affect the major organs of the body. Nanomedicine recently emerged as a better option for the treatment of these deadly diseases. As a result, many nanoparticles have been used to treat cancer cell lines. Of the various nanoparticles, zinc oxide exhibits biocompatibility. Therefore, the aim of the present study was to investigate the activity of zinc oxide nanoparticles (ZnO-NPs) against HepG2 and MCF-7 cells. The NPs (~13 ± 2 nm) were prepared via a non-protonated chemical route and were well-characterized through standard techniques. The study showed that treatment with NPs is notably effective against the proliferation of HepG2 and MCF-7 cancer cells in a dose-dependent manner. The MTT (3-(4,5-dimethyl thiazol-2-yl)-2,5-diphenyl tetrazolium bromide, a tetrazole) assays revealed the concentration-dependent cytotoxic effects of NPs in range of 2.5–100 μg/ml. HepG2 and MCF-7 cells were exposed to ZnO-NPs and exhibited a significant reduction in their cell viability (95% and 96%; $p < 0.05$) in response to a very low concentration (25 μg/ml) of the ZnO-NPs; this finding was confirmed with FACS (fluorescence-activated cell sorting) data. The reduction in cell viability in response to NP treatment induces cytotoxicity in the cultured cells. The quantitative RT-PCR (real-time polymerase chain reaction) results demonstrate that the exposure of HepG2 cells to ZnO-NPs results in significant upregulation of the mRNA expression level of Bax, p53, and caspase-3 and the down regulation of the anti-apoptotic gene Bcl-2. The NPs were also tested against five pathogenic bacteria through the disk diffusion method, and their antibacterial activities were compared with that of ZnO salt.

1. Introduction

Nanobiotechnology/bionanotechnology, which is the fastest emerging field of material science, connects several branches of basic sciences, including biology, chemistry, biotechnology, mathematics material science, and engineering. The technology develops nanofabricated materials with a very small diameter (1–100) to manipulate and transform various types of biological systems [1–9]. Bionanotechnology exhibits vast applications because it is largely used in cosmetics, skin care products, drug delivery, nanomedicines, cancers, molecular biology, markers, tissue engineering products, non-viral gene carriers, clinical bio-analytical diagnostics, and therapeutics because chemotherapy, radiation, and surgery were the old techniques used to reduce cancers [1–10]. Of the wide range of applications of nanobiotechnology, it is widely applied to reduce cancers with the use of inexpensive inorganic nano-scale materials. Nanomaterials, which have very small diameter (~30 nm), exhibit unique physicochemical characteristic due to their size; these include a high surface area, low cost, enhanced reactivity, ability to easily enter cells, and ability to affect various types of biological systems [1–12]. It is known that cancer is a heterogeneous and complex disease that occurs when the normal cell proliferation controls are lost. The positive/normal cells change into cancer cells through three distinct phases, i.e., initiation, promotion, and progression. Several reports have reported the toxicity of nanostructures, which kill human cancerous cells and are very useful for protection against cancers [13–15]. Of the various types of cancers, hepatocellular carcinoma is the fourth most common malignant tumour in the world [16,17]. The incidence

* Corresponding author at: College of Science, Department of Zoology, P.O. Box 2455, King Saud University, Riyadh 11451, Saudi Arabia. Tel.: +966 5360 23284.
E-mail address: rwahab05@gmail.com (R. Wahab).

http://dx.doi.org/10.1016/j.colsurfb.2014.02.038
0927-7765/

of this disease is very high in many countries, such as the United States, United Kingdom, Japan, and China. The mortality rate associated with this disease ranks second in China among all tumours. Another prevalent cancer is breast cancer, which is commonly diagnosed among females. Millions of women are fighting from breast cancer worldwide, and this disease corresponds to more than one-fifth of the global cancer burden. Several developed and developing countries are affected ranging from an age-parameter such as 20.7 in Uganda to 90.7 in the USA per 100,000 [18]. In Europe, this rate is higher, i.e., 421,000 cases of breast cancer were estimated in 2008 [19]. A total 184,450 new breast cancer cases appeared during the period of 2008–2011 [20]. Several therapies, such as chemotherapy, radio therapy, and immune therapy, have been adopted to protect against this cancer, but the outcome rates remain negligible [21,22]. In a new scientific scenario, various types of nanostructures, such as the nanostructures of metal oxides, particularly zinc oxide (ZnO), which is popularly known as a family of nanostructures, have received much attention because of their low cost, effectiveness, and vast applications in various fields, such as photo-catalysis, sunscreen, cosmetic products, optoelectronics, solar cells, sensors, piezoelectric, light emission, and antibacterial agents [11,21–24]. The semiconductor metal oxides (ZnO), which function well for reflecting light, require that the particle size of ZnO, among others materials (e.g., alumina, ceria, and zirconia), be approximately 20–50 nm. ZnO (3.37 eV) has a band gap similar to that of TiO_2 (3.23 eV) and can thus easily enter human cells. In enzyme and protein solutions, Zn^{2+} ions play a vital role by creating ionic signals among various intra- and intercellular organelles. It also interacts with proteins, and free Zn^{2+} ions can cause cytotoxicity [25,26]. The various-shaped nano and microstructure of ZnO, which are capped with multiple-sized nanospikes, imitate filopodia cells and can target HSV-1 pathogenesis [27]. Antoine et al. [28] demonstrated that the zinc oxide tetrapod-like structures synthesised via a flame process have the capacity to block the entry and spread of the HSV-2 virus into target cells [28]. The prepared tetrapod ZnO nanostructures have the ability to neutralise HSV-2 virions [28]. The benefits of using an inorganic nanomaterial compared to an organic material include that the inorganic nanomaterial is stable, easy to fabricate, less toxic, heat-resistant, and sufficiently durable in the absence of light exposure [26,29]. The development of methods to prepare NPs with reduced toxicity will be useful for various applications, such as cell imaging, drug delivery, and cancer therapy [14,15]. The present study was designed to investigate the cytotoxicity of well-characterised ZnO-NPs and their effects on the cancer HepG2 (liver cancer) and MCF-7 (breast cancer) cells. The HepG2 cell line was selected because liver cancer is a major health problem worldwide [30,31]. The zinc oxide NPs were used as the target material to reduce the number of cancer cells. In this study, we investigated the detailed characterization of the prepared NPs. The cell viability and apoptosis in presence of NPs were analysed through the *MTT* assay and flow cytometry, respectively. The data were consistent with the *RT-PCR* analysis. The prepared NPs were also tested against five pathogens, and the results obtained using the disk diffusion method revealed that the NPs achieved good inhibition of microbial strains compared with zinc salt.

2. Experimental

2.1. Materials and methods

2.1.1. Synthesis of zinc oxide nanoparticles (ZnO-NPs)

The NPs of ZnO were successfully synthesised with the use of zinc acetate dihydrate ($Zn(Ac)_2{\cdot}2H_2O$) and p-xylene ($C_6H_4(CH_3)_2$). The solution was prepared in 100 ml of MeOH under constant stirring. In a typical experiment, the zinc salt (0.3 M) was first diluted in 100 ml of MeOH, and the mixture stirred for 30 min for complete dissolution of the zinc salt. p-Xylene (20 ml) was then poured into the mixture, and the pH of the solutions (Thermo Scientific, UK) was measured until it reached ~6.76. The stirred solution was transferred to a three-necked refluxing pot, refluxed at ~65 °C for 6 h, and cooled to room temperature. The transparent solution changed to a white suspension after 5 h of reflux, but the complete precipitate was achieved after 6 h. The chemicals used for the preparation of NPs ($(Zn(Ac)_2{\cdot}2H_2O)$ and p-Xylene ($C_6H_4(CH_3)_2$) were purchased from Aldrich Chemical Co. Ltd. and used without further purification. The organic impurities were removed from the solution via centrifugation for 10 min at 4000 rpm/min (FLETA 5, Hamlin Science and Industrial Co. Ltd, U.K.). The obtained white precipitate was washed with methanol and dried on a Petridish at room temperature. The obtained white powder sample was characterised in terms of its morphological, chemical, and optical properties.

2.2. Characterization of NPs

The obtained NPs were characterised using the standard characterisation tools. For example, the morphology was observed via FESEM (field emission scanning electron microscopy) and TEM (transmission electron microscopy, Jeol JSM-2010, Japan) as described in our previously published papers [23,24]. The crystallinity of the NPs was observed with XRD (X-ray diffraction pattern, Rigaku, Japan) and $Cu_{K\alpha}$ radiation ($\lambda = 1.54178$ Å) with a Bragg angle ranging from 20° to 65° at a 6° min^{-1} scanning speed. The chemical composition of the synthesised powder was characterised through FTIR spectroscopy in the range of 4000–400 cm^{-1}. Additionally, the optical properties of the sample were also analysed using a UV-Visible spectrophotometer (Shimazu) in the range of 200–600 nm at room temperature.

2.3. Cell culture

HepG2 and MCF-7 cells were grown in DMEM/MEM culture medium supplemented with 10% foetal bovine serum (FBS), 0.2% sodium bicarbonate, and an antibiotic–antimycotic solution (100×, 1 ml/100 ml of medium). The cells were grown in a humidified environment with 5% CO_2 and 95% atmosphere at 37 °C. Prior to use in the experiments, the cells were assessed to determine their cell viability using the Trypan blue dye exclusion assay following the manufacturer's protocol, and only those batches [32] showing a viability of more than 95% were in the study. HepG2 and MCF-7 cells were used between passages 10 and 12 for the NP treatments.

2.4. Reagents and consumables

MTT and all of the specified chemicals were purchased from Sigma Chemical Company Pvt., Ltd. (St. Louis, MO, USA). DMEM and MEM culture media, the antibiotics-antimycotic solution, and foetal bovine serum were purchased from Invitrogen (USA). The culture wares and other plastic consumables used in the study were procured commercially from Nunc (Denmark).

2.5. MTT assay

The percent cell viability was assessed using the MTT assay with the following protocol [33]. In brief, the cells (1×10^4) were seeded in 96-well culture plates and allowed to adhere for 24 h under a high-humidity environment with 5% CO_2 and 95% O_2 atmosphere at 37 °C. The cells were then exposed to various concentrations (2.5–100 μg/ml) of NPs for 24 and 48 h. After exposure, MTT (5 mg/ml of stock in PBS) was added (10 μl/well of 100 μl of cell suspension), and the plate was incubated for 4 h. At the end of the incubation period, the reaction mixture was carefully removed,

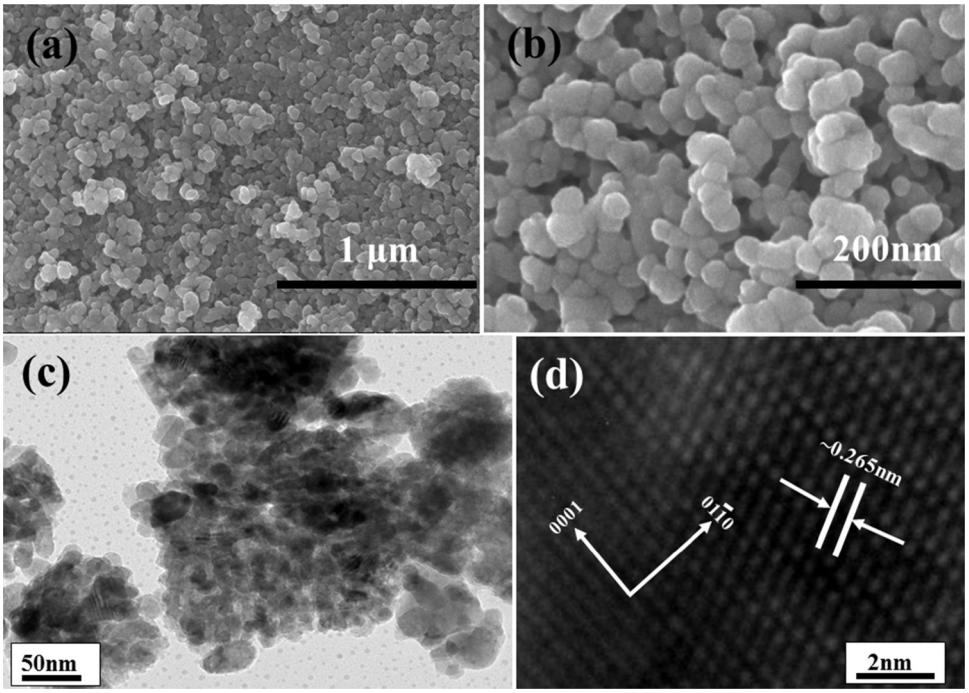

Fig. 1. FESEM and TEM images of ZnO-NPs. (a) Low-magnification FESEM image; (b) high–magnification FESEM image. (c) Low-magnification TEM image of the ZnO-NPs synthesised at ~65 °C; (d) high-magnification TEM image showing the distance between two lattice fringes, which is approximately 0.265 nm.

and 200 μl of DMSO was added to each well and mixed gently. The plates were maintained on a rocking shaker for 10 min at room temperature, and the absorbance was read at 550 nm using a multi-well micro-plate reader (Multiskan Ex, Thermo Scientific, Finland). Untreated sets were also run under identical conditions and served as the controls.

2.6. Flow cytometry

2.6.1. Flow cytometric analysis of cell cycle progression

MCF-7 and HepG2 cells treated with Milli-Q (control) and ZnO-NPs (at concentrations ranging from 2.5 to 100 μg/ml and 5 to 25 μg/ml, respectively) for 24 respectively were harvested and centrifuged at 3600 × *g* for 5 min. The pellets were resuspended in 500 μl of ice-cold 70% ethanol and incubated at 4 °C for 1 h. After two successive washes with PBS with centrifugation at 3600 × *g* for 5 min, the cell pellets were resuspended in PBS and stained with 50 μg/ml of propidium iodide (PI) containing 0.1% Triton X-100 and 0.5 mg/ml RNAase for 1 h at 30 °C in dark. The fluorescence of the PI was measured by flow cytometry using a Beckman Coulter flow cytometer (Coulter Epics XL/Xl-MCL, Miami, USA) through a FL-4 filter (585 nm), and 10,000 events were acquired [34]. The data were analysed using the Coulter Epics XL/XL-MCL System II software (version 3.0). The cell debris characterised by a low FSC/SSC was excluded from the analysis.

2.7. Total RNA isolation and quantitative real-time PCR analysis of apoptotic markers

For the isolation of the total RNA, HepG2 cells were cultured in six-well plates and exposed to ZnO-NPs at a concentration of 100 μg/ml for 24 h. At the end of the exposure period, the total RNA was extracted using an RNeasy Mini kit (Qiagen) according to the manufacturer's instructions. The concentration of the extracted RNA was determined using a Nanodrop 8000 spectrophotometer (Thermo-Scientific), and the integrity of the RNA was visualised on a 1% agarose gel using a gel documentation system (Universal Hood II, BioRad). The first-strand cDNA was synthesised from the total RNA by reverse transcription using the oligo-p(dT)12–18 primer and MLV reverse transcriptase (GE HealthCare, UK). The following sets of specific primers were employed for the amplification of each cDNA: p53, caspase 3, Bax, and BCl_2. The expression levels were normalised to the expression level of the HPRT gene, which was used as an internal housekeeping control. Real-time quantitative PCR (qRT-PCR) was performed using the Quanti Tect SYBR Green PCR kit (Qiagen) in a Light Cycler® 480 instrument with a 96-well plate (Roche Diagnostics, Rotkreuz, Switzerland). The results were obtained from three subsamples, and the PCR assay was repeated twice for each sample. A relative quantification analysis was performed using the Roche LightCycler®480 software (version 1.5). The mRNA expression level normalised to that of the HPRT gene was calculated, and the data were subjected to a statistical analysis to identify any significant differences between the cells treated with ZnO-NPs and the untreated control cells.

2.8. Antibacterial activity of zinc salt and the prepared ZnO-NPs

The salt of zinc oxide (zinc acetate dihydrate ($Zn(Ac)_2{\cdot}2H_2O$) and the prepared NPs of zinc oxide were tested to determine their antimicrobial activities against *E. coli*, *S. aureus*, *P. aeruginosa*, *B. subtilis*, and *S. acidaminiphila.* In a typical experiment, the pathogenic bacteria were maintained on nutrient broth media in a Petri dish, and after solidification of the agar layer, ~10-mm wells were cut from the agar layer using a sterile 1-ml micropipette tip. Then, 200 μl of each solution of ZnO salts and the prepared ZnO-NPs were poured into the wells. The control solution was used to check the formation of colonies. The plates were incubated overnight at 37 °C, and the colonies were counted. After incubation, the diameters of the inhibition zone (mm) were measured, and the percentage survival was determined. The percent survival of the cells treated with the zinc salt was compared with that of the cells treated with the prepared NPs.

Table 1
Calculation of the particle size of the ZnO-NPs from the FWHM of the X-ray diffraction pattern.

S.N.	Peak position	FWHM (in rad)	$\cos\theta$	Particle size (nm)
ZnO-NPs	31.69°	0.0123	0.9622	11.63
	34.33°	0.0101	0.9554	14.30
	36.17°	0.0102	0.9507	11.54

3. Results and discussion

3.1. Morphological study of grown NPs by FESEM and TEM analysis

Fig. 1a and b shows the morphology of the grown NPs through FESEM at low and high magnifications, respectively. At lower magnification, it is very clear that the obtained NPs are spherical in shape (Fig. 1a) and are found as aggregated particles. In contrast, Fig. 1b shows the high-magnification image of the prepared ZnO-NPs. These images demonstrate that the average size of the individual NPs is approximately 13 ± 2 nm. To clarify the average size of the NPs and their morphology, the powder sample was further analysed through TEM with selected area electron diffraction (SAED) patterns. Fig. 1c shows a low-magnification TEM image of the ZnO-NPs that is clearly consistent with the size of the NPs determined through the FESEM observations and reveals that the grown ZnO-NPs are spherical in shape. The size of each NP obtained was in the range of ~13–15 nm. Moreover, the NPs exhibit smooth and clean surfaces. Fig. 1d shows a high-resolution TEM (HR-TEM) image of the NPs. The lattice fringes are separated by ~0.265 nm, which is equal to the lattice constant of ZnO and indicates that the obtained structure exhibits a wurtzite phase.

3.2. X-ray diffraction pattern (XRD)

The crystalline nature of the grown powder was analysed based on its X-ray diffraction pattern (Fig. 2a) under the above-described conditions. The spectra clearly show that the diffraction peaks in the pattern are indexed at the ZnO with lattice constants $a = 3.249$ and $c = 5.206$ Å and are well matched with the available Joint Committee on Powder Diffraction Standards (JCPDS 36-1451). No other peaks related to impurities were detected in the spectra within the detection limit of the X-ray diffraction instrument, which further confirms that the synthesised powder is pure ZnO. The crystallinity of the obtained ZnO-NPs increases with an increase in the intensity of the ⟨1 0 1 0⟩, ⟨0 0 0 2⟩, and ⟨1 0 1 1⟩ peaks. The particle size of the ZnO-NPs was calculated using the well-known Scherer formula [35] with the FWHM of the X-ray diffraction pattern, and the value of the peak position is shown in Table 1. The calculation was performed using a Gaussian and Lorentzian fitting program. The average value of the particle sizes was ~13 nm.

3.3. FTIR spectroscopy and chemical reaction mechanism of synthesised ZnO-NPs

The functional quality of the product was analysed through FTIR spectroscopy. The spectrum was acquired in the range of 400–4000 cm^{-1} (Fig. 2b). The signal of the ZnO band was observed at 427 cm^{-1} [36,37]. The bands at 3200–3600 cm^{-1} correspond to the O–H mode of vibration. The C=O stretching mode of vibration was observed at 1597 cm^{-1} and 1354 cm^{-1}, and these peaks are related to C=O and C–O, respectively [36,37]. The synthesised powder was also analysed using a UV–visible spectrophotometer at room temperature to determine the optical properties of the material. A broad band was observed in the spectrum at 351 nm

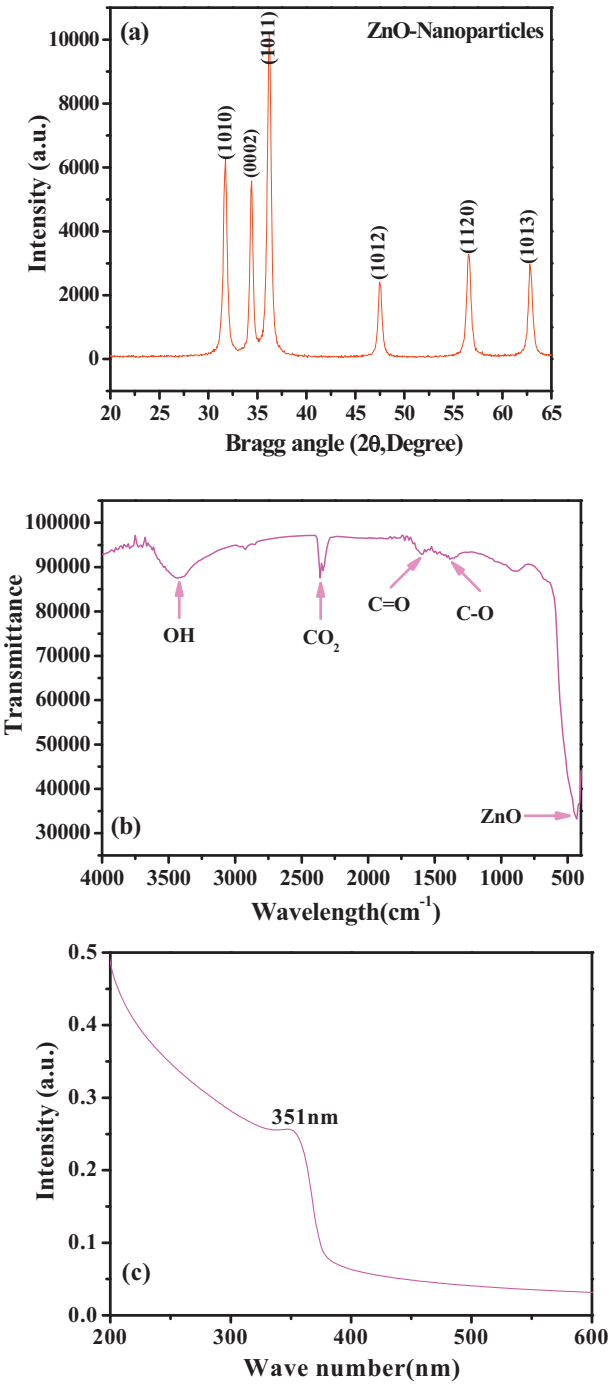

Fig. 2. (a) X-ray diffraction pattern, (b) FTIR spectrum, and (c) UV-–vis spectrum of grown ZnO-NPs.

(3.53 eV, very close to the band gap of pure ZnO (3.37 eV), which is a characteristic band for wurtzite, hexagonal, pure ZnO. No other peak was observed in the spectrum, which again confirms that the synthesised products are pure ZnO (Fig. 2c) [36,37].

Based on the above-described characterisations, such as the X-ray diffraction pattern, FESEM, TEM, FTIR, and UV–visible spectroscopy, we propose a brief mechanism for the formation of the spherical-shaped ZnO-NPs. As described in Section 2.1, a solution of p-xylene (20 ml mixed with MeOH (80 ml)) was added to the source material of the NPs (zinc acetate dihydrate ($Zn(Ac)_2 \cdot 2H_2O$)) under continuous stirring with methanol as the solvent. The solution appeared clear without any precipitate at pH ~6.76 and was

transferred to the refluxing pot and refluxed at 65 °C. As the refluxing time increased, a white precipitate started to form until it was completed formed after 6 h. Under these conditions, we may assume that the hydrogen bond between –CH_3 (alkyl group) ($C_6H_4(CH_3)_2$) reacts with the acetate group of zinc acetate to form the zinc complex C_6H_4Zn and methyl ethanoate (CH_3COOCH_3) (Eq. (1)). An increase in the reflux time of this solution increases the amount of solvent (MeOH) that directly reacts with the formed complex (C_6H_4Zn) to form $Zn(OH)_2$ and regenerate xylene (Eq. (2)). Zinc hydroxide ions exist in the solution as the ionic forms Zn^{2+} and $2OH^-$ (Eq. (3)). At a higher refluxing temperature, the zinc and hydroxyl (OH^-) ions change into pure zinc oxide (ZnO) and water (Eq. (4)). The by-product water molecule from the reaction is leached out during the centrifugation and drying processes [23,24]. It is assumed that the initially formed $Zn(OH)_2$ in the solution result in the aggregation of nuclei and that the acquisition of sufficient thermal energy from the refluxing pot leads to the formation of small active molecules of ZnO. These initial or active ZnO nuclei/particles are expected to be the building blocks for the formation of the spherical-shaped ZnO-NPs [23,24].

$$Zn(CH_3COO)_2 \cdot 2H_2O + C_6H_4(CH_3)_2 \xrightarrow{CH_3OH} C_6H_4Zn + 2CH_3COOCH_3 \quad (1)$$

$$C_6H_4Zn + 2CH_3OH \rightarrow Zn(OH)_2 + 2C_6H_4(CH_3)_2 \quad (2)$$

$$Zn(OH)_2 \rightarrow Zn^{2+} + 2OH^- \quad (3)$$

$$Zn^{2+} + 2OH^- \rightarrow ZnO + H_2O \quad (4)$$

3.4. Microscopic observation of HepG2 and MCF-7 cancer cells with ZnO-NPs

The proliferation of the cancer HepG2 and MCF-7 cells in the presence of various concentrations (2.5–100 μg/ml) of the prepared ZnO-NPs was observed through microscopy after different incubation (24 and 48 h) periods. Fig. 3 shows the proliferation of HepG2 cancer cells and their interactions with different concentrations of ZnO-NPs (Fig. 3a). The data clearly show that the cells were mononucleated on day 1; however, when the cells reached nearly 50% confluence and were treated with various concentrations of the prepared NPs, the cell density was reduced due to their interaction with the NPs in a dose-dependent manner. No significant change was observed at the NP concentrations of 2.5 and 5 μg/ml, but an increase in the concentration of the NPs from 10 to 25 μg/ml reduced the growth of the cancer cells. The cells were completely damaged at the two highest concentrations (50 μg/ml and 100 μg/ml) of nanoparticles (Fig. 3b). The same observations were also made for MCF-7 cells treated with the prepared NPs (Fig. 4a).

3.5. Zinc oxide nanoparticle-induced cytotoxicity (MTT assay)

The MTT solution is largely used to determine the viability of cells and leads to mitochondrial dysfunction [38]. The yellow MTT is reduced into a purple formazan salt in the mitochondria of living cells. Consequently, a solubilisation buffer solution (usually dimethyl sulphoxide (DMSO)) was added to dissolve the insoluble purple formazan product into a colored solution. The absorbance of the colored solution was then quantified by a spectrophotometer at a certain wavelength (usually ~550–570 nm). The absorption maximum depends on the solvent employed, and the percentage (%) viability is calculated according to the following equations:

$$\%\,\text{viability} = \left[\frac{(\text{total cells} - \text{viable cells})}{\text{total cells}}\right] \times 100$$

Or

$$\%\,\text{viability} = \frac{\text{OD(optical densities) in sample well}}{\text{OD in control well}} \times 100$$

HepG2 and MCF-7 cells were exposed to ZnO-NPs (2.5–100 μg/ml) for 24 and 48 h, and the cytotoxicity was measured by MTT assays. The obtained results show that the cell viability was reduced by the ZnO-NPs and that the degree of reduction was concentration/dose-dependent. As determined through the MTT assay, the HepG2 cell viability was observed at 24 h 99%, 97%, 59%, 8%, 6%, and 5% (Fig. 3a and b) and at 48 h 97%, 97%,47%,5%, 4%, and 3% in response to treatment with 2.5, 5, 10, 25, 50, and 100 μg/ml NPs, respectively ($p < 0.05$ for each); in contrast, the MCF-7 cell viability was observed at 24 h 94%, 93%, 92%, 7%, 6%, and 4% and at 48 h to 91%, 87%, 79%, 4%, 3%, and 3% (Figs. 4a and 4b). The data obtained from the HepG2 and MCF-7 cells treated with NPs are clearly consistent with the microscopic observations (Figs. 3a and 4a).

3.6. Evaluation of the death of various cancer cells

3.6.1. Death of MCF-7 cells induced by ZnO-NPs

MCF-7 cells treated with ZnO-NPs (100 μg/ml) exhibited significant induction of apoptosis, as determined by the appearance of almost 26% of the cells in the sub G1 phase of the cell cycle compared with 2.8% cells of the untreated control cells (Fig. 5a). Compared with the untreated control, 20% and 23.1% increases in the percentage of cells in the G2/M phase were observed after treatment with 25 and 50 μg/ml NPs, and these numbers gradually declined to 11% with treatment with 100 μg/ml ZnO-NPs. Compared to the untreated control. MCF-7 cells treated with NPs as concentrations of 25, 50, and 100 μg/ml also exhibited significant decline of 5.8%, 6.7%, and 8.8% cells in the normal G1 phase (Fig. 5b). Treatment with ZnO-NPs at the lower doses of 2.5–10 μg/ml did not result in any significant changes in the cell cycle of MCF-7 cells.

3.6.2. Death of HepG2 cells induced by ZnO-NPs

HepG2 cells treated with 25 μg/ml ZnO-NPs exhibited induction of apoptosis, as evidenced by the appearance of a significant increase in the number of cells in sub G1 phase (12.2%) compared with the 8.4% cells that were observed in the untreated control (Fig. 6a). HepG2 cells treated with 25 μg/ml ZnO-NPs exhibited a significant 38.9% increase in the number of cells in the G2 M phase compared to 28.8% of the cells in the control population. At the concentration of 25 μg/ml, a significant decline of 24% in the number of HepG2 cells in the G1 phase was observed (Fig. 6b). Treatment with ZnO-NPs at the lower doses of 5 and 10 μg/ml did not result in any significant changes in the cell cycle of HepG2 cells.

3.7. RT-PCR results

In this study, quantitative real-time PCR was utilised to analyse the mRNA levels of apoptotic markers (e.g., p53, Bax, bcl-2, and caspase-3) in HepG2 cells exposed to ZnO-NPs at a concentration of 50 μg/ml for 24 h. The results showed that the mRNA levels of these apoptotic markers were significantly altered in HepG2 cells due to ZnO-NP exposure (Fig. 7, $p < 0.05$ for each). The mRNA level of the tumour suppression gene p53 was 1.9-fold higher and the mRNA expression levels of the pro-apoptotic gene Bax and the anti-apoptotic gene bcl-2 were decreased (2.7- and 2.5-fold, respectively) in the exposed cells compared with the untreated cells. Moreover, we examined the effect of ZnO-NPs on the mRNA expression level of caspase-3 and found that it was 1.8-fold higher in the treated cells compared with the untreated control cells. We analysed the mRNA expression levels of the p53, Bax, bcl-2, and caspase levels in HepG2 cells in response to ZnO-NP

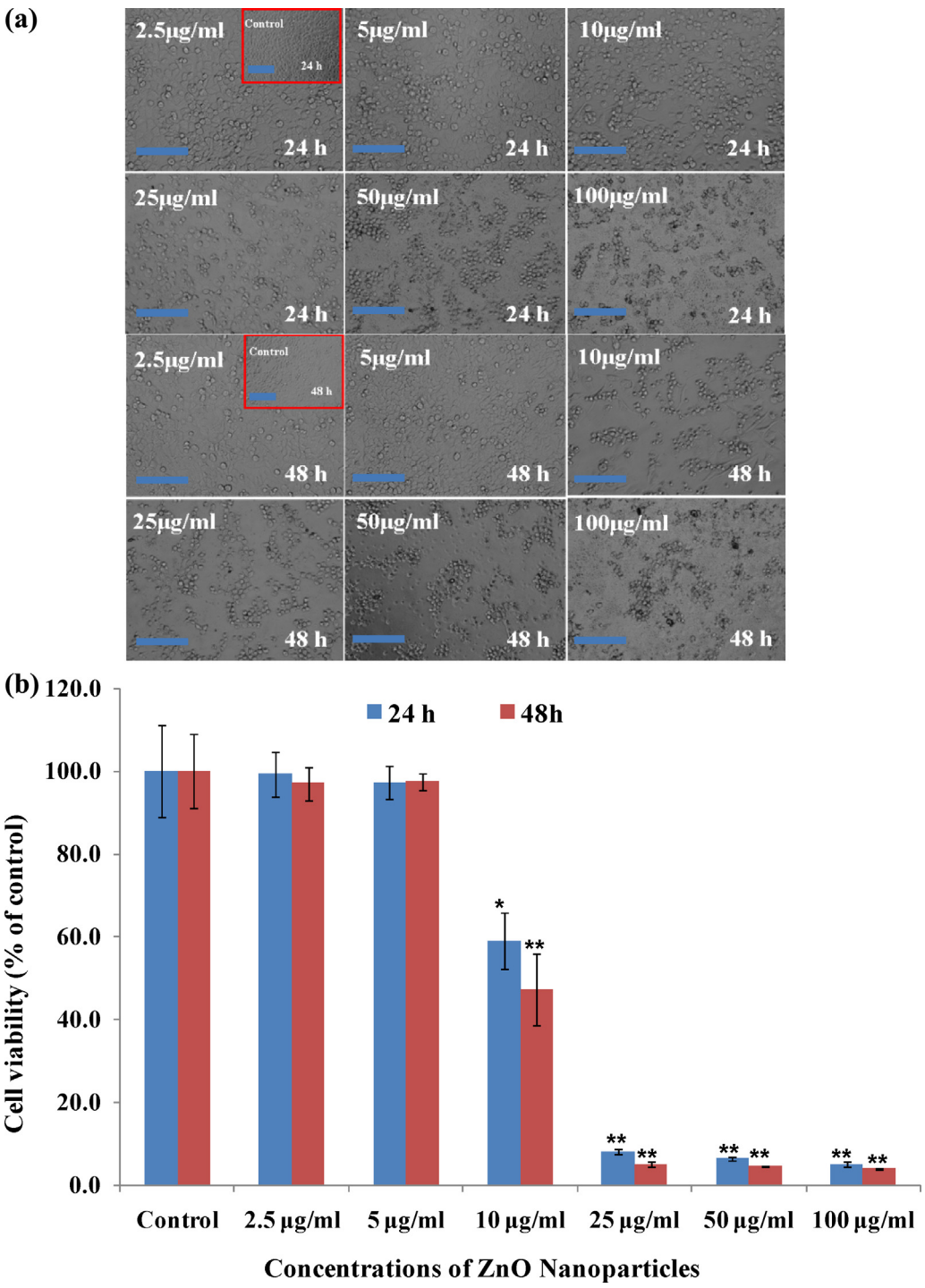

Fig. 3. (a) Microscopic images of HepG2 cells after treatment with ZnO-NPs for 24 and 48 h, (b) Mitochondrial activity (assessed by the MTT assay) in HepG2 cells exposed to various concentrations of ZnO-NPs for 24 and 48 h. The values are the mean ± SD of three independent experiments. *$p < 0.01$ and **$p < 0.001$ vs. the control group (each scale bar = 1 mm).

exposure because apoptosis is controlled through these pathways. The quantitative real-time PCR results show that the ZnO-NPs upregulate the mRNA levels of the cell cycle checkpoint protein p53 and the pro-apoptotic protein Bax. The expression of the anti-apoptotic protein bcl-2 was downregulated in cells exposed to ZnO-NPs. Furthermore, the upregulation of p53 and the down-regulation of bcl-2 family members, such as Bax, induces the permeabilisation of the outer mitochondrial membrane, which releases soluble proteins from the intermembrane space into the cytosol, where they promote caspase activation [39,40].

3.8. Antibacterial study

The bactericidal activities of the zinc oxide salt and the prepared ZnO-NPs against the tested pathogens were tested using the agar diffusion technique. The results, which are shown in Table 2, demonstrate that the prepared ZnO-NPs result in good zone inhibition against *E. coli, S. aureus, P. aeruginosa, B. subtilis*, and *S. acidaminiphila*, as determined after the cultures are incubated at 37 °C overnight and the colonies were counted. The results show that the best zone inhibition against *E. coli* (22 mm), *P. aeruginosa*

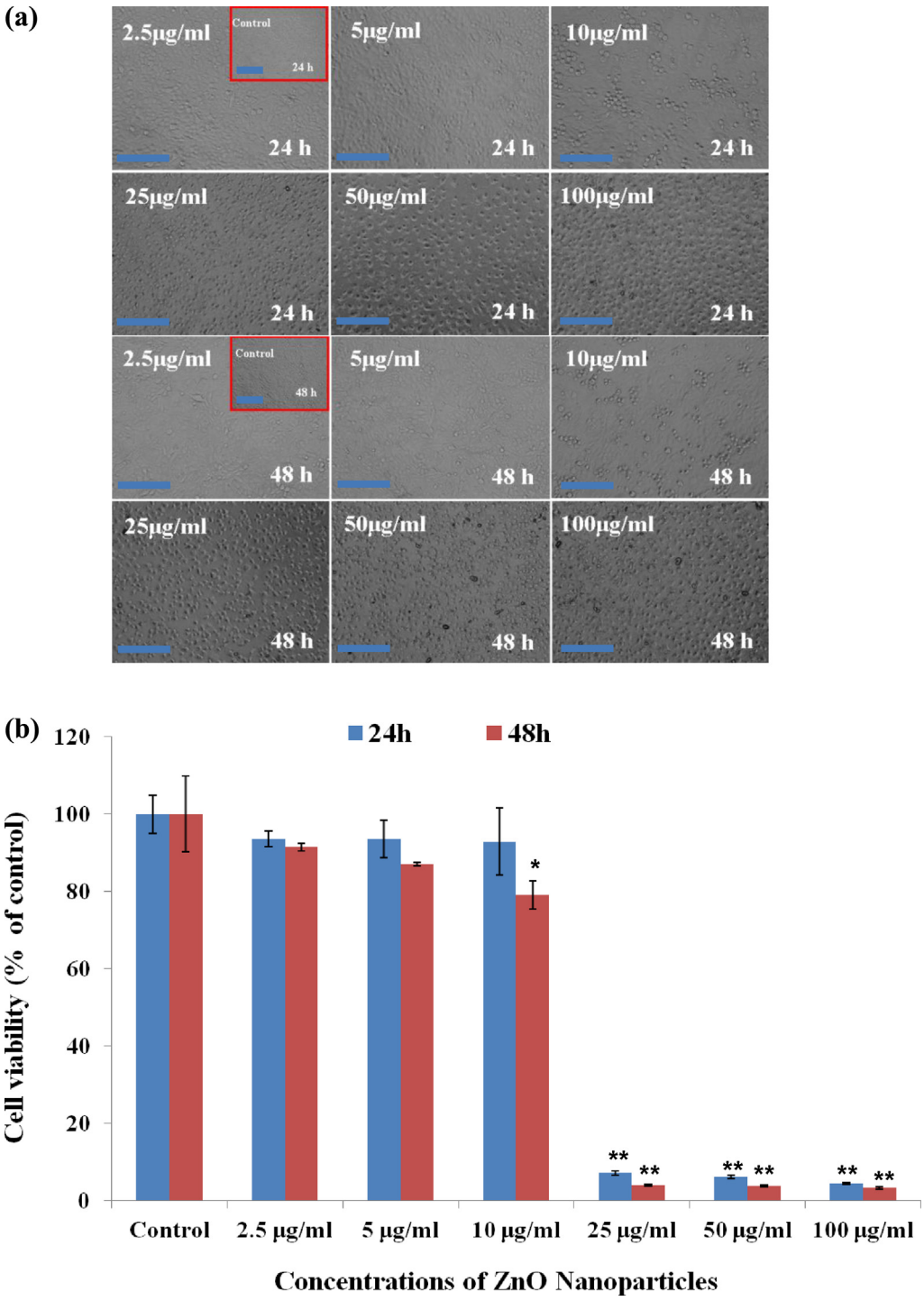

Fig. 4. (a) Microscopic images of MCF-7 cells after treatment with ZnO-NPs for 24 and 48 h, (b) Mitochondrial activity (assessed by the MTT assay) in MCF-7 cells exposed to various concentrations of ZnO-NPs for 24 and 48 h. The values are the mean ± SD of three independent experiments. $^{*}p < 0.01$ and $^{**}p < 0.001$ vs. the control group (each scale bar = 1 mm).

(20 mm), *S. aureus* (17 mm), *S. acidaminiphila* (18 mm), and *B. subtilis* (16 mm) is obtained with the NPs. In contrast, the tested ZnO salt showed lower inhibition rates compared with the ZnO-NPs (Table 2) against the five pathogens. The data show the zone inhibition results obtained with the ZnO salt against *E. coli* (12 mm), *S. aureus* (10 mm), *P. aeruginosa* (8 mm), *B. subtilis* (8 mm), and *S. acidaminiphila* (7 mm). The NPs of ZnO, which have a very small diameter (~13 ± 2 nm), can easily attach to and enter the inner surface of the microorganisms. The size of each microorganism is approximately 200–250 fold higher than that of the prepared NPs, which allows them to easily form a film and easily pass through the cell wall of the microorganisms. The NPs of ZnO react with the cytoplasm of the microorganisms due their high surface area and chemical stability, causing its destruction and ultimately leading to the death of the cell [22–24,41].

Based on the chemical and biological results, we may assume that the NPs of ZnO act as cheap anticancer drugs against the cancer HepG2 and MCF-7 cells. We may also postulate the physical

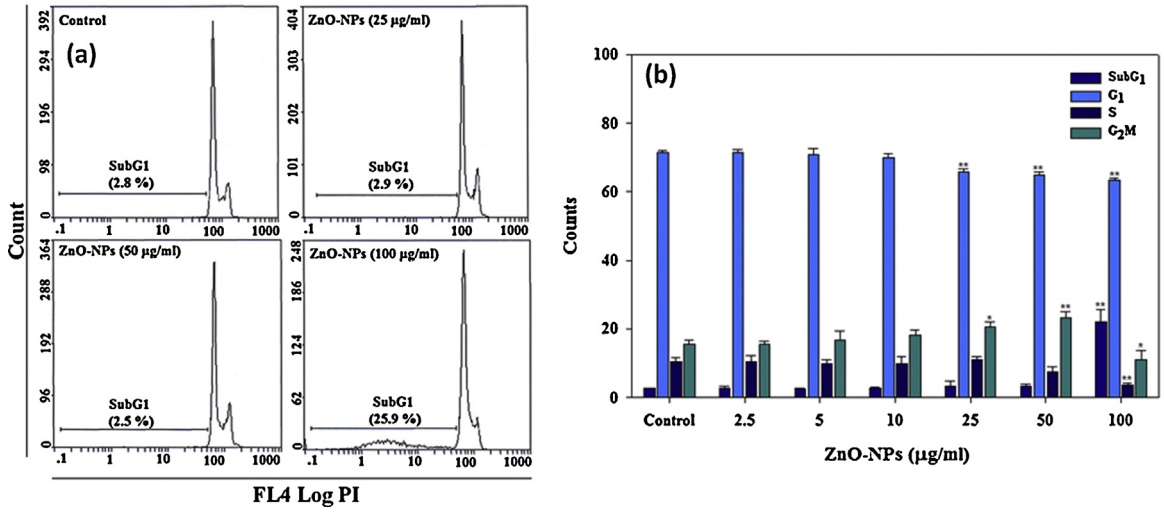

Fig. 5. (a) Cell cycle analysis of PI-stained nuclei of MCF-7 cells. Representative FACS images showing the changes in the progression of the normal cell cycle as a function of the ZnO-NP concentration are shown. $SubG_1$, which was analysed using a biomarker, represents the percentage of cells that underwent apoptosis/necrosis, (b). Flow cytometric analysis of the cell cycle progression of MCF-7 cells exposed to ZnO-NPs for 24 h. Each histogram represents the mean ± SD from three independent experiments. $^{*}p < 0.05$ and $^{**}p < 0.01$ compared with the control, as determined by one-way ANOVA. G_1, S, and G_2/M represent the percentages of cells in the normal phases of the cell cycle, and $SubG_1$ represents the percentage of cells that underwent apoptosis/necrosis.

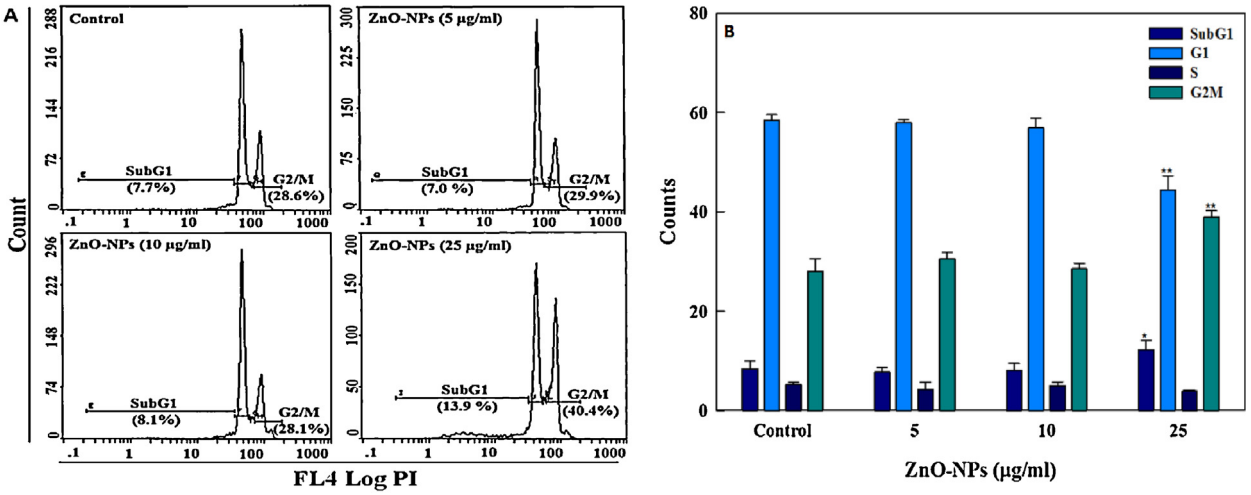

Fig. 6. (a) Cell cycle analysis of PI-stained nuclei of HepG2 cells. Representative FACS images exhibiting the changes in the progression of the normal cell cycle as a function of the ZnO-NP concentration are shown. The SubG1 and G2 M phases, which were analysed using biomarkers, represent the percentage of cells that underwent apoptosis/necrosis and cell cycle arrest, respectively. (b) Flow cytometric analysis of the cell cycle progression of HepG2 cells exposed to ZnO-NPs for 24 h. Each histogram represents the mean ± SD from three independent experiments. $^{*}p < 0.05$ and $^{**}p < 0.01$ compared to the control group, as determined by one-way ANOVA. G_1, S, and G_2/M represent the percentages of cells in the normal phases of the cell cycle, and $SubG_1$ represents the percentage of cells that underwent apoptosis/necrosis.

mechanism, as described in Section 2.1: spherical-shaped ZnO-NPs entered the cancer cells in a dose-dependent manner after incubation for the desired periods (24 and 48 h). In this study, the NPs first attached to the outer membrane and then penetrate into the cancer cell layer. The cells have small pores that help the NPs enter into the inner membrane. The prepared NPs are able to enter into cells (~20 μm) very easily due to their very small size (~13 ± 2 nm) compared to the size of cells [42,43]. The high density of the small NPs in the liquid system strongly favours the rapid formation of agglomerates, and it is assumed that these agglomerates of ZnO-NPs destroy cellular cell organelles, such as DNA, RNA, endoplasmic reticulum, and mitochondria [43]. The aggregation appears to be a ubiquitous phenomenon among all nanoparticles [44]. In this study, we showed that the small ZnO-NPs can be endocytosed by cells and form aggregates inside the cell, resulting in cytotoxicity [44]. The addition of the ZnO nanoparticles to cell lines may result in cell death depending on the size of the nanomaterials. The cell death may depend on the cell type, experimental procedures, concentrations, efficiency of the cellular uptake, and duration of exposure [45–47]. In effect, our findings show that the efficiency of the cellular uptake of ZnO-NPs and the resultant intracellular concentration may be responsible for the cytotoxicity of ZnO-NPs at higher

Table 2
Zone of inhibition of bacterial growth of *E. coli, S. aureus, P. aeruginosa, B. subtilis*, and *S. acidaminiphila* with increasing concentrations of ZnO-NPs or zinc salt ($Zn(Ac_2)\cdot 2H_2O$. The data represent the mean ± SD of three experiments.

Bacterial strain	Zone of inhibition (mm)	
	$Zn(Ac)_2\cdot 2H_2O$	ZnO-NPs
Escherichia coli	12 ± 1	22 ± 2
Staphylococcus aureus	10 ± 1	17 ± 1.5
Pseudomonas aeruginosa	8 ± 0.3	20 ± 0.57
Bacillus subtilis	8 ± 1	16 ± 0.6
Stenotrophomonas acidaminiphila	7 ± 0.3	18 ± 0.55

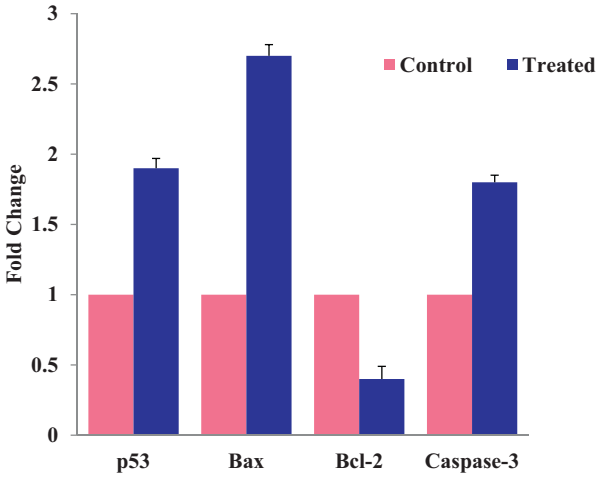

Fig. 7. Effect of ZnO-NPs on mRNA expression levels of apoptotic markers in HepG2 cells. The cells were treated with ZnO-NPs at a concentration of 50 μg/ml for 24 h. Quantitative real-time PCR was performed using the Roche LightCycler®480 software (version 1.5). The HPRT gene was used as the internal control to normalise the data. The data are presented as the mean ± SD of three identical experiments with three replicates. *Significantly different compared with the control group ($p < 0.05$ for each).

concentrations. An increase in the concentration of the NPs in the cell suspension result in more NPs attaching to the cells walls and entering the cytoplasm to react with and destroy an increasing number of cellular organelles, which leads to cell death. ROS (reactive oxygen species) are another factor because it produced in cells with NPs and are responsible for the formation of free radicals that penetrate the outer walls of the cells and enter the inner wall of the membrane. These free radicals react with the cellular organelles to cause enzymatic changes and promote the disorganisation of the cellular contents. Oxidative stress plays an important role in the toxicity of NPs, and it is suggested that the extreme generation of ROS through NPs reduces the cellular antioxidant capacity [48,49]. The mechanism through which ZnO-NPs are responsible for the regulation of the growth or destruction of cellular organelles and their biochemical and enzymatic changes in cancer cells is under investigation, and further study is required to investigate the role of ZnO-NPs in HepG2 and MCF-7 cancer cells [43]. Most previous toxicity studies have employed metal oxide nanostructures at a high concentration, and it is thus difficult to assess the effect of human exposure. We hypothesise that the use of ZnO-NPs, which are biocompatible at lower concentrations, would be helpful for the control of the growth of cancer cells and would have no adverse effect on the body [50]. Additionally, the prepared ZnO-NPs were also tested in an antibacterial study against five pathogens, namely *E. coli*, *S. aureus*, *P. aeruginosa*, *B. subtilis*, and *S. acidaminiphila*, via the disk diffusion method, and their antibacterial potential was compared with that of zinc salt. The results show that the NPs are more potent against bacteria than the salt of zinc oxide (Table 2), and this effect may be due to the size of the nanoparticles, which are very small and can easily enter through the bacterial membrane [23,24].

4. Conclusions

In summary, the prepared nanoparticles of zinc oxide were successfully synthesised via a soft chemical solution process. The NPs were characterized in terms of their chemical and optical properties using standard characterization tools, such as XRD, FESEM, TEM, UV–vis spectroscopy, and FTIR spectroscopy. The NPs were used at a very low concentration and were found to exhibit activity against HepG2 and MCF-7 cancer cells in a dose-dependent manner. The results of the antiproliferative studies clearly demonstrate that treatments with NPs sensitise cancer cells. The degree of apoptosis was found to be enhanced with an increase in the concentration of NPs, and a significant concentration of NPs resulted in cellular death in both cell lines. The importance of the present study lies in the possibility that the next-generation NPs may be more efficacious as antiproliferative agents. However, a detailed investigation of these NPs and their stability under biological conditions is required. The results of our study demonstrate that ZnO-NPs induce cytotoxicity and apoptosis in HepG2 and MCF-7 cancer cells, and this effect is likely mediated through ROS generation and oxidative stress. The NPs were also tested against *E. coli*, *S. aureus*, *P. aeruginosa*, *B. subtilis*, and *S. acidaminiphila* through the disk diffusion method and achieved a higher reduction in bacterial proliferation than did the control treatment.

Acknowledgment

The financial support provided by the National Plan for Sciences and Technology (NPST Project No. 12-NAN2490-02) of King Saud University in Riyadh is greatly acknowledged.

References

[1] M.N. Rittner, Am. Ceram. Soc. Bull. 81 (2002) 33.
[2] E. Oesterling, N. Chopra, V. Gavalas, X. Arzuag, E.J. Lim, R. Sultana, D.A. Butterfield, L. Bachas, B. Hennig, Toxicol. Lett. 178 (2008) 160.
[3] J.M. Laval, P.E. Mazeran, D. Thomas, Analyst 125 (1999) 29.
[4] T.A. Desai, Med. Eng. Phys. 22 (9) (2000) 595.
[5] L.A. Bauer, N.S. Birenbaum, G.J. Meyer, J. Mater. Chem. 14 (2004) 517.
[6] L. Mazzola, Nat. Biotechnol. 21 (2003) 1137.
[7] K.M. Reddy, K. Feris, J. Bell, D.G. Wingett, C. Hanley, A. Punnoose, Appl. Phys. Lett. 90 (2007) 213902.
[8] H.H. Wang, C.S. Xie, W. Zhang, S. Cai, Z. Yang, Y. Gui, J. Hazard. Mater. 141 (2007) 645.
[9] Z.J. Han, I. Levchenko, S. Kumar, M.M.A. Yajadda, S. Yick, D.H. Seo, P.J. Martin, S. Peel, Z. Kuncic, K. Ostrikov, J. Phys. D: Appl. Phys. 44 (17) (2011) 174019.
[10] S.I. Stupp, Chem. Rev. 105 (4) (2005) 23.
[11] S.S. Hong, T.H. Joo, I.I.W. Park, Y.H. Jun, G.C. Yi, Appl. Phys. Lett. 83 (2003) 4157.
[12] J. Schulz, H. Hohenberg, F. Pflucker, E. Gartner, T. Will, S. Pflucker, R. Wepf, V. Wen del, H. Gers-Barlag, K.P. Wittern, Adv. Drug Deliv. Rev. 54 (2002) S157.
[13] H.S. Nalwa, T. Webster, Cancer Nanotechnology-Nano materials for Cancer Diagnosis and Therapy, Ameri. Scie. Pub, Los. Angeles, 2007.
[14] M.I. Khan, A. Mohammad, G. Patil, S.A. Naqvi, L.K. Chauhan, I. Ahmad, Biomaterials 33 (5) (2012) 1477.
[15] M. Ahamed, M.J. Akhtar, M. Raja, I. Ahmad, M.K.J. Siddiqui, M.S. AlSalhi, S.A. Alrokayan, Nanomed. Nanotechnol. Biol. Med. 7 (2011) 904.
[16] M. Sherman, Semin. Oncol. 28 (2001) 450.
[17] Q.H. Ye, L.X. Qin, M. Forgues, P. He, J.W. Kim, A.C. Peng, R. Simon, Y. Li, A.I. Robles, Y. Chen, Z.C. Ma, Z.Q. Wu, S.L. Ye, Y.K. Liu, Z.Y. Tang, X.W. Wang, Nat. Med. 9 (4) (2003) 416.
[18] S. Pecorelli, G. Favalli, L. Zigliani, F. Odicino, Int. J. Gynaecol. Obstet. 82 (2003) 369.
[19] J. Ferlay, D.M. Parkin, E. Steliarova-Foucher, Eur. J. Cancer 46 (2010) 765.
[20] C. Desantis, R. Siegel, P. Bandi, A. Jemal, Cancer J. Clin. 61 (6) (2011) 4009.
[21] L.M. Davids, B. Kleemann, Cancer Treat. Rev. 37 (2011) 465.
[22] G.M. Murphy, Photoimmunol. Photomed. 15 (1999) 34.
[23] R. Wahab, A. Mishra, S.I. Yun, Y.S. Kim, H.S. Shin, Appl. Microb. Biotechnol. 87 (2010) 1917.
[24] R. Wahab, Y.S. Kim, A. Mishra, S.I. Yun, H.S. Shin, Nanoscale Res. Lett. 5 (2010) 1675.
[25] C.J. Frederickson, J.Y. Koh, A.I. Bush, Nat. Rev. Neurosci. 6 (2005) 449.
[26] C.J. Frederickson, M.D. Hernan-dez, S.A. Goik, J.D. Morton, J.F. McGinty, Brain Res. 446 (1988) 383.
[27] Y.K. Mishra, R. Adelung, C. Röhl, D. Shukla, F. Spors, V. Tiwari, Antiviral Res. 92 (2011) 305.
[28] T.E. Antoine, Y.K. Mishra, J. Trigilio, V. Tiwari, R. Adelung, D. Shukla, Antiviral Res. 96 (2012) 363.
[29] D. Bechet, P. Couleaud, C. Frochot, M.L. Viriot, F. Guillemin, M. Barberi-Hey ob, Trends Biotechnol. 26 (2008) 612.
[30] A. Nel, T. Xia, L. Madler, N. Li, Science 311 (2006) 622.
[31] M. Ott, V. Gogvadze, S. Orrenius, B. Zhivotovsky, Apoptosis 12 (2007) 913.
[32] M.A. Siddiqui, M.P. Kashyap, V. Kumar, A.A. Al-Khedhairy, J. Musarrat, A.B. Pant, Toxicol. In Vitro 24 (2010) 1592.
[33] M.A. Siddiqui, G. Singh, M.P. Kashyap, V.K. Khanna, S. Yadav, D. Chandra, A.B. Pant, Toxicol. In Vitro 22 (2008) 1681.
[34] Q. Saquib, S.M. Attia, M.A. Siddiqui, M.A.M. Aboul-Soud, A.A. Al-Khedhairy, J.P. Giesy, J. Musarrat, Toxicol. Appl. Pharm. 259 (1) (2012) 54.
[35] B.D. Cullity, Elements of X-ray Diffraction, Addison-Wesley, Reading, MA, 1978.

[36] R. Wahab, S.G. Ansari, Y.S. Kim, M.W. Song, H.S. Shin, Appl. Surf. Sci. 255 (2009) 4891.
[37] R. Wahab, S.G. Ansari, Y.S. Kim, H.K. Seo, G.S. Kim, G. Khang, H.S. Shin, Mater. Res. Bull. 42 (2007) 1640.
[38] T. Mosmann, J. Immunol. Methods 65 (1–2) (1983) 55.
[39] F.P. Pablo, S.S. Guy, Biochem J 384 (2004) 201.
[40] R.J. Youle, A. Strasser, Nat. Rev. Mol. Cell Biol. 9 (1) (2008) 47.
[41] J.M. Yousef, E.N. Danial, J. Health Sci. 2 (4) (2012) 38.
[42] E. Chang, N. Thekkek, W.W. Yu, V.L. Colvin, R. Drezek, Small 12 (2006) 1412.
[43] L.K. Limbach, Y. Li, R.N. Grass, T.J. Brunner, M.A. Hintermann, M. Muller, D. Gunther, W.J. Stark, Environ. Sci. Technol. 39 (23) (2005) 9370.
[44] W. Cui, J. Li, Y. Zhang, H. Rong, W. Lu, L. Jiang, Nanomed. Nanotechol. Biol. Med. 8 (1) (2012) 46.
[45] R. Foldbjerg, P. Olesen, M. Hougaard, D.A. Dang, H.J. Hoffmann, H. Autrup, Toxicol. Lett. 190 (2) (2009) 156.
[46] S. Arora, J. Jain, J.M. Rajwade, K.M. Paknikar, Toxicol. Lett. 179 (2) (2008) 93.
[47] N. Asare, C. Instanes, W.J. Sandberg, et al., Toxicology 291 (1–3) (2012) 65.
[48] M. Ahamed, M.S. AlSalhi, M.K.J. Siddiqui, Clin. Chim. Acta 411 (2010) 1841.
[49] J.P. Wise, B.C. Goodale, S.S. Wise, Aquat. Toxicol. 97 (2010) 34.
[50] S.M. Hussain, J.J. Schlager, Toxicol. Sci. 108 (2009) 223.